ACS OMEGA

Article

Cite This: ACS Omega 2019, 4, 14589−14598

http://pubs.acs.org/journal/acsodf

Electronic, Electrical, and Magnetic Behavioral Change of SiO_2-NP-Decorated MWCNTs

James A. Oke,[†] David O. Idisi,[†] Sweety Sarma,[†] Sabata J. Moloi,[†] Sekhar C. Ray,*[,†] Kuan Hung Chen,[‡] Anirudha Ghosh,[‡] Abhijeet Shelke,[‡] and Way Faung Pong*[,‡]

[†]Department of Physics, CSET, University of South Africa, Private Bag X6, Florida, 1710, Science Campus, Christiaan de Wet and Pioneer Avenue, Florida Park, Johannesburg, South Africa

[‡]Department of Physics, Tamkang University, Tamsui 251, Taipei, Taiwan

ABSTRACT: Silicon-oxide-nanoparticle (SiO_2-NP) heteroatoms were decorated/deposited onto multiwall carbon nanotube (MWCNT) surface to tune the properties of MWCNTs for electronic and magnetic applications. To achieve this objective, SiO_2-NPs and MWCNTs were prepared and suspended together into toluene and heated at <100 °C for the formation of MWCNTs/SiO_2-NP nanocomposites. A change in the microstructure, electronic, electrical, and magnetic behaviors of MWCNT nanocomposites decorated/deposited with silicon content was investigated using different techniques, viz., scanning electron microscopy, X-ray diffraction, Raman spectroscopy, and X-ray photoelectron spectroscopy for structural, compositional, and electronic structure, while current−voltage was used for electrical properties and field-dependent magnetization and electron spin resonance techniques were used for magnetic properties. The results indicated that SiO_2-NPs adhered onto MWCNTs, resulting in variation in the material conductivity with the Si-NP content. The coercivity of MWCNT nanocomposites adhered with 1.5 atom % Si-NPs (H_C@40 K = 689 Oe) is higher than that of those adhered with 5.75 atom % Si-NPs (H_C@40 K = 357 Oe). In general, the results provide information about the possibilities of tuning the electronic, electrical, and magnetic properties of MWCNTs by adherence of SiO_2-NPs onto them. This tuning of material properties could be useful for different electronic and magnetic device applications.

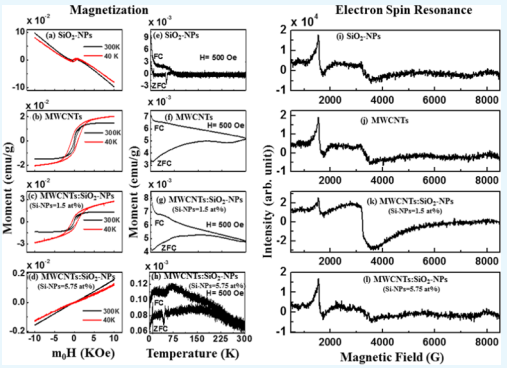

1. INTRODUCTION

Since their discovery in 1991,[1] single-walled and multiwalled carbon nanotubes (CNTs) have been materials of choice for a variety of applications due to their unique physical and electrical properties. The materials also possess properties that make them suitable for fabrication of electrochemical sensors.[2] Despite their potential for these applications, electronic, electrical, and magnetic properties of CNTs need to be tailored for more different device-based applications. Over few decades, significant progress has been made by various researchers in exploring graphitic carbon materials such as graphene, fullerene, and CNTs owing to their unique properties for different applications.[3−5] Zhang et al. explored the CNT semiconductor composites and other carbon materials for photocatalytic properties and their results showed a significant activity.[5] Other studies also showed the possibility of tuning the properties of multiwalled carbon nanotubes (MWCNTs) by introducing heteroatoms like nitrogen and boron.[6]

Theoretical studies have shown that in CNTs, Si atoms relax outward and form a sp^3 bonding to change the electronic and magnetic behaviors of the material.[7] Silicon (Si) atoms chemisorb on the surface of CNTs to provide dangling bonds that change the properties of the material for different applications in addition to the known ones.[2,6] Silicon atoms can be binding centers for various atoms or molecules, making CNTs easier and more attractive for functionalization.[8] Silicon, therefore, could be a preferred element to functionalize CNTs due its large atomic size, which distorts the host lattice to generate/induce defects in the material.

In comparison to other dopants like nitrogen and boron, effects of silicon on properties of CNTs have not been fully explained nor understood. In comparison to theoretical studies, there is scarce experimental data presented on CNTs deposited with Si nanoparticles (NPs). In the present study, MWCNTs are a material of interest because they have better properties than graphene and fullerene. Although they have similar properties, graphene is a semiconductor with a zero forbidden gap,[9] while CNTs are metallic or semiconductor with the forbidden gap ranging from 0 to 2 eV.[10,11] The technique used in the production of CNTs has control over its length, diameter, and morphology,[12] which have a great influence in tailoring their properties for preferred applications. On the other hand, fullerene is a single-wall CNT (SWCNT) with closed ends and have similar properties to those of MWCNTs. The advantage of MWCNTs over SWCNT is that

Received: June 29, 2019
Accepted: August 9, 2019
Published: August 26, 2019

DOI: 10.1021/acsomega.9b01958
ACS Omega 2019, 4, 14589−14598

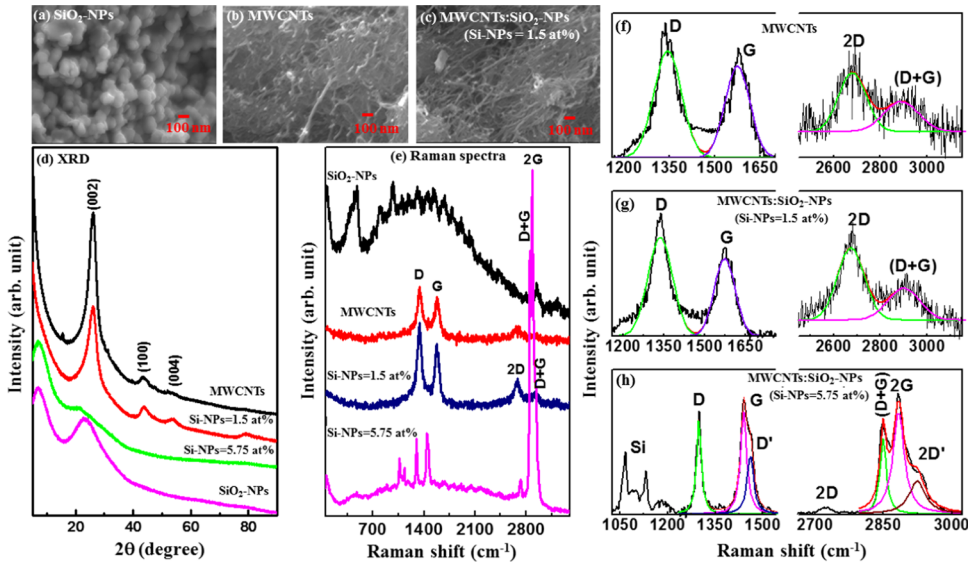

Figure 1. Scanning electron microscopy of (a) SiO_2-NPs, (b) MWCNTs, and (c) MWCNTs/SiO_2-NPs (Si-NPs = 1.5 atom %). (d) X-ray diffraction pattern, (e) Raman spectra for Si-NPs, MWCNTs, MWCNTs/SiO_2-NP (Si-NPs = 1.5 atom %) nanocomposites, and MWCNTs/SiO_2-NP (Si-NPs = 5.75 atom %) nanocomposites. First-order and second-order deconvoluted Raman spectra for (f) SiO_2-NPs, (g) MWCNTs, (h) MWCNTs/SiO_2-NP (Si-NPs = 1.5 atom %) nanocomposites, and (i) MWCNTs/SiO_2-NP (Si-NPs = 5.75 atom %) nanocomposites.

there is a possibility to produce them in large quantity;[12] hence, we studied MWCNTs. We have synthesized MWCNT and deposited different concentrations of Si-NPs on MWCNTs and studied their structural, electronic, electrical, and magnetic properties using different spectroscopic techniques. The Si-NPs got oxidized during the synthesis process to form silicon-oxide-nanoparticles (SiO_2-NPs) and adhered onto MWCNTs. Our motivation is that due to the adherence of Si-NPs, MWCNTs are a potential candidate for ferromagnetic and electromagnetic nanodevice applications. This motivation is based on the data acquired using different material research techniques.

2. RESULTS AND DISCUSSION

2.1. Surface Morphology. Surface morphologies of SiO_2-NPs, MWCNTs, and MWCNTs/SiO_2-NP (Si-NPs = 1.5 atom %) nanocomposites are shown in Figure 1a–c. Figure 1a shows small aggregates of SiO_2-NPs, with size distribution varying from 50 to 100 nm. Figure 1b clearly indicates the formation of MWCNTs with a uniform diameter with little contamination, while Figure 1c confirms the decoration/deposition of SiO_2-NPs on the surface of MWCNTs as indicated in the tree-buds-like structure on the anchored branches. It can also be seen from the figure that SiO_2-NPs are well-dispersed and bounded to the surface of MWCNTs. This attachment and anchoring of SiO_2-NPs to the surface of MWCNTs is important for the variation of the electrical conductivity of MWCNTs and for the prevention of an aggregation behavior of SiO_2-NPs during the whole charging/discharging process among Si@C/CNTs (mixture of Si@C and CNTs) and oxygen. This variation of conductivity is shown later in the text. However, it is noted that as they were exposed to air, the Si-NPs were oxidized during the synthesis process to form SiO_2-NPs on the surface of MWCNTs.

2.2. X-Ray Diffraction. Figure 1d shows the X-ray diffraction (XRD) spectra for all the synthesized nanocomposites. The spectrum for MWCNTs show a prominent peak at $2\theta \approx 26°$ corresponding to the (002) plane of the graphitic structure[13] and less intense peaks at $2\theta \approx 44$ and 53° corresponding to the (100) and (004) reflection,[13] respectively. This structure matches with that of pristine MWCNTs and/or standard graphite carbon, indicating a well-graphitized MWCNTs[14] without carbonaceous impurities and/or catalytic metal particles on the surface of the MWCNTs. The adherence of 1.5 atom % Si onto MWCNTs results in an additional peak at $2\theta \approx 78°$ corresponding to the (110) plane[15] along with the (002), (100), and (004) planes, indicating that the structure of MWCNT is still intact. However, when oxidized Si-NPs (5.75 atom %) is adhered onto MWCNTs, these peaks disappeared, resulting in two peaks at lower angles of $2\theta \approx 22$ and 7°. We assume that these two peaks may arise from SiO_2/Si−O−C and Si−Si structures respectively.[16,17] Casati et al. found a peak at $2\theta \approx 6.5°$ in $AlSi_{10}Mg$ alloy and claimed that the peak arises from silicon and is a reflection of Si (111),[16] whereas the peak at $2\theta \approx 22°$ is consistent with crystalline SiO_2 as previously reported by Svavarsson et al.[17]

2.3. Raman Spectroscopy. Figure 1e shows the Raman spectra of the synthesized SiO_2-NPs, MWCNTs, and their nanocomposites. A wide peak at ∼520 cm^{-1} observed for SiO_2-NPs is attributed to the Si peak.[18] In the case of MWCNTs, four main peaks observed at approximately 1345, 1585, 2693, and 2937 cm^{-1} correspond to the D-band (disordered graphitic), G-band, 2D-band, and (D + G)-band, respectively.[19−23] The D-peak is due to defected graphite.[19−23] The G-peak, on the other hand, has been found to be due to the doubly degenerate zone centered around the E_{2g} mode resulting from the stretching modes of C−C bonds of typical graphite[19] The 2D peak is an overtone of the D peak and occurs due to a second-order vibration process, and the D + G-peak occurs due to the combined vibration of D and G modes. These four peaks were also observed when different oxidized Si-NPs concentrations (1.5 and 5.75 atom %) were decorated/deposited on the MWCNTs surface and are found to be shifted slightly toward a lower wavelength for MWCNTs/SiO_2-NPs (Si-NPs = 1.5 atom %). In the case of MWCNTs/SiO_2-NPs (5.75 atom %), a peak representing SiO_2 is observed

DOI: 10.1021/acsomega.9b01958
ACS Omega 2019, 4, 14589−14598

in addition to four carbon peaks of MWCNTs. The existence of a SiO_2 peak in the Raman spectra indicates that Si-NPs were oxidized to form SiO_2-NPs on the surface of MWCNTs (Table 1). The peak may also be due to the relatively high concentration of silicon atom onto MWCNTs. Thus, the measurements may also confirm that SiO_2-NPs have been deposited on MWCNTs matrices. Presumably, the shift in the peak positions is consistent with the shift in the XRD spectra, implying the formation of the MWCNTs/SiO_2-NP nanocomposites. Due to the large surface area of silicon,[24] the atom can easily create a bond length stretching, which leads to a significant softening effect of the MWCNT/SiO_2-NP composites.[25] The adherence of silicon also induces a low-frequency shift of the MWCNTs spectrum. The first- and second-order Raman spectra deconvoluted into two Gaussian lines for MWCNTs and MWCNTs/SiO_2-NPs (Si-NPs = 1.5 atom %) and three Gaussian lines for MWCNTs/SiO_2-NP (Si-NPs = 5.75 atom %) nanocomposites are shown in Figure 1f–h. The evaluated peak intensities (int.), peak widths ($\Delta\omega$), and peak positions (x) of the deconvoluted spectra are presented in Table 2. It can be seen from the table that the peak widths of D- and G-bands are low (narrow) for MWCNTs/SiO_2-NP composites. The narrowing of the peak width is due to reduction of defects as a result of substitutional SiO_2 atoms. To understand the degree of crystallization of the nanocomposites, I_D/I_G ratio was calculated from the deconvoluted Raman peaks. The I_D/I_G ratios are 1.3, 1.5, and 0.74 for MWCNTs, MWCNTs/SiO_2-NPs (Si-NPs = 1.5 atom %), and MWCNTs/SiO_2-NPs (Si-NPs = 5.75 atom %), respectively. The variation of the ratio indicates the degree of disordered carbon atoms in the nanocomposites.[19−23,26] The high ratio (I_D/I_G) of the nanocomposites indicates a structural change of the composites. In MWCNTs, SiO_2-NPs change the crystal structure of the composites. We have estimated the crystallite size using the Tuinstra−Koenig relation[27]

$$L_a\ (\mathrm{nm}) = \frac{4.4}{R}\left(\frac{2.41}{E_1}\right)^4$$

where the energy difference "R" is the integrated intensity ratio I_D/I_G and E_1 is the excitation laser energy (≈2.33 eV). The crystallite size of MWCNTs/SiO_2-NP (Si-NPs = 5.75 atom %) nanocomposite is higher than that of pure MWCNTs as tabulated in Table 1. A change in L_a is due to oxidized silicon atoms relaxing outward and forming a sp^3 bond[7] in the MWCNTs/SiO_2-NP nanocomposite. This conjecture is in good agreement with the XRD results as discussed above.

2.4. X-Ray Adsorption Near Edge Spectroscopy. The C K-edge X-ray adsorption near edge spectroscopy (XANES) spectrum in Figure 2a shows that there is a transition from C 1s core to p-like final states above the Fermi level (E_f). The spectrum also shows the π^* features that are associated with sp^2-bonding configurations at ∼285.5 (±0.1) eV[28,29] and σ^* features at ∼292.8 eV. The π^* region was subtracted within the range of 284−289 eV using a Gaussian line and is shown as an inset in Figure 2a. The inset shows double structural features centered at ∼285.5 (±0.1) and 287.1 eV for MWCNTs and MWCNTs/SiO_2-NP nanocomposites, respectively. The intensity of pure MWCNT is found to be higher than that of MWCNT/SiO_2-NP (Si-NPs = 5.75 atom %) and lower than the intensity of MWCNTs/SiO_2-NPs (Si-NPs = 1.5 atom %). As suggested elsewhere,[30] these features in the π^* region may indicate that C−H or Si−C(:H) or Si−C(:O) and sp^2 C−C

Table 1. Compositional/Quantificational Analysis from XPS, Crystallite Size from XRD, and (I_D/I_G) Ratio from Raman Spectra of SiO_2-NPs, MWCNTs, MWCNTs/SiO_2-NPs (Si-NPs = 1.5 atom %), and MWCNTs/SiO_2-NPs (Si-NPs = 5.75 atom %)

	compositional and quantificational analysis from XPS			wt % of oxidized Si-NPs on MWCNTs surface obtained from XPS	(I_D/I_G) ratio	L_a (nm) from XRD	L_a (nm) from Raman
	C (atom %)	O (atom %)	Si (atom %)				
SiO_2-NPs		63.60	36.40				
MWCNTs	98.37	01.63			1.3	2.8	3.8
MWCNTs/SiO_2-NPs (Si-NPs = 1.5 atom %)	94.00	4.50	1.50	3.42	1.5	2.6	3.4
MWCNTs/SiO_2-NPs (Si-NPs = 5.75 atom %)	85.0	9.25	5.75	12.15	0.74	5.1	6.8

DOI: 10.1021/acsomega.9b01958
ACS Omega 2019, 4, 14589−14598

Table 2. Different Parameters Obtained after De-Convolution of Raman Spectra of SiO_2-NPs, MWCNTs, MWCNTs/SiO_2-NPs (Si-NPs = 1.5 atom %), and MWCNTs/SiO_2-NPs (Si-NPs = 5.75 atom %)

	x (cm^{-1})	$\Delta\omega$ (cm^{-1})	int. (au)	x (cm^{-1})	$\Delta\omega$ (cm^{-1})	int. (au)	x (cm^{-1})	$\Delta\omega$ (cm^{-1})	int. (au)
First Order Raman Spectra	Peak-I (D-band)			Peak-II (G-band)			Peak-III D′-band		
MWCNTs	1343	92	2.1	1574	82	1.6			
MWCNTs/SiO_2-NPs (Si-NPs = 1.5 atom %)	1336	91	3.9	1573	77	2.6			
MWCNTs/SiO_2-NPs (Si-NPs = 5.75 atom %)	1298	18	2.8	1439	23	3.8	1460	24	2.4
Second Order Raman Spectra	(2D-band)			(D + G)-band			(2G-band/2D′-band)		
MWCNTs	2679	118	0.7	2888	150	0.5			
MWCNTs/SiO_2-NPs (Si-NPs = 1.5 atom %)	2673	116	1.4	2900	138	0.7			
MWCNTs/SiO_2-NPs (Si-NPs = 5.75 atom %)	2727	38	1.5	2924	43	14.2	2850	16	12.3
							2873	30	29.9

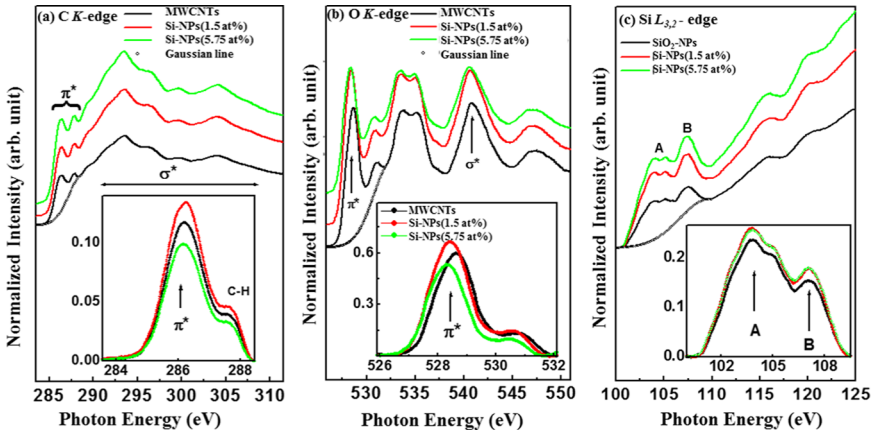

Figure 2. X-ray absorption near edge structure (XANES) spectroscopy for MWCNTs, MWCNTs/SiO_2-NPs, and SiO_2-NPs: (a) C K-edge, (b) O K-edge, and (c) Si-$L_{3,2}$-edge.

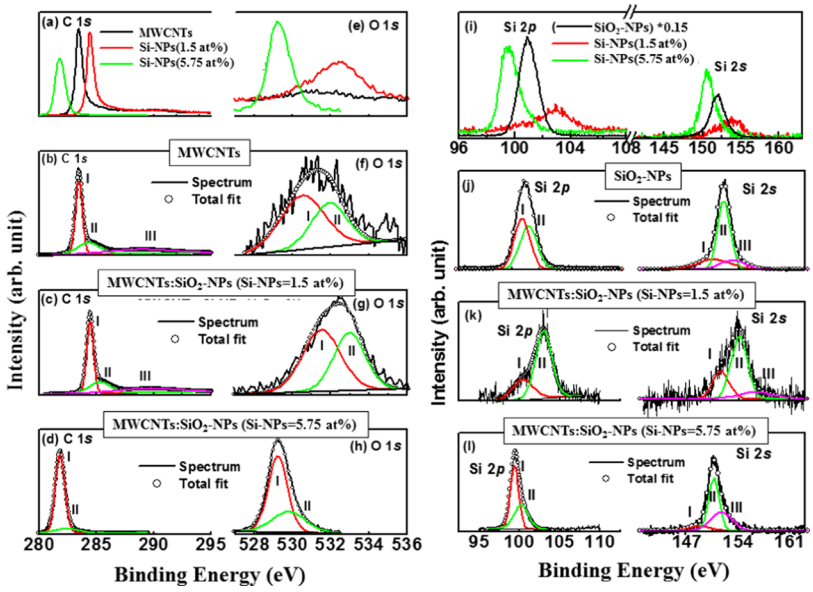

Figure 3. (a) C 1s and (e) O 1s XPS spectra for MWCNTs, MWCNTs/SiO_2-NP (1.5 atom %) nanocomposites, and MWCNTs/SiO_2-NP (5.75 atom %) nanocomposites. Deconvoluted C 1s (b–d) and O 1s (f–h) XPS spectra for MWCNTs, MWCNTs/SiO_2-NP (Si-NPs = 1.5 atom %) nanocomposites, and MWCNTs/SiO_2-NP (Si-NPs = 5.75 atom %) nanocomposites. (i) Si 2p XPS spectra and (j–l) deconvoluted Si 2p XPS of Si-NPs, MWCNTs/SiO_2-NP (Si-NPs = 1.5 atom %) nanocomposites, and MWCNTs/SiO_2-NP (Si-NPs = 5.75 atom %) nanocomposites.

bonds have been formed. Effects of Si–C(:H) and/or Si–C(:O) bonding on the electronic structure of MWCNTs is confirmed by the difference in the intensities of the nanocomposites. These results indicate that the MWCNTs changes the near-edge unoccupied C 2p states upon SiO_2-NPs decoration/deposition on the surface of MWCNTs, causing their structural/electronic properties to change. The normalized O K-edge XANES spectra of the nanocomposites in Figure 2b show several peaks at ∼529 and ∼531 eV and a double structure at ∼533/∼535 eV in the π^* region. The

DOI: 10.1021/acsomega.9b01958
ACS Omega 2019, 4, 14589−14598

origin of the peaks at ~529 and ~531 eV is attributed to bond resonance transitions from carboxylic groups and hydroxyl groups.[31] The observed double structure peaks at ~533 and 535 eV in each O K-edge spectra were assigned to the physisorbed O_2[32] that may occur during the nanocomposite synthesis process. The peak at ~540.5 eV for MWCNTs is assigned to σ^*[30] and is shifted to ≈0.4 eV toward the lower energy for MWCNTs/SiO_2-NPs, indicating that the oxidized Si-NPs interacted with C and O in MWCNTs. The subtracted background shown as an inset of Figure 2b indicates that the intensity of MWCNTs is higher than that of MWCNTs/SiO_2-NPs (Si-NPs = 5.75 atom %) and lower than that of MWCNTs/SiO_2-NP (Si-NPs = 1.5 atom %) nanocomposites. This variation of intensities indicates that O 2p and Si 3p states are coupled in MWCNTs/SiO_2-NPs. Figure 2c shows the normalized Si $L_{3,2}$-edge XANES spectra of SiO_2-NPs and MWCNTs/SiO_2-NP composites. Spectral features, A and B, in Figure 2c for MWCNTs and MWCNTs/SiO_2-NPs are separated by ~2.0 eV. Feature A shows a splitting of 1.0 eV, indicating a poor resolved features at ~104 and 105 eV.[33] The double split of A might be a spin−orbit doublet due to the transition of Si $2p_{3/2}$ and $2p_{1/2}$ core states to the antibonding Si 3s derived states.[33] The feature B, on the other hand, can be explained in terms of the Si 2p-to-3p transition and/or is associated with the resulted Si 3s or 3d derived states from hybridization with O 2p orbitals.[33,34] Both spectral features are shifted slightly toward the lower energy, indicating that the electronic structure of MWCNTs changed due to the incorporation of SiO_2-NPs in the MWCNTs matrice.

2.5. X-Ray Photoelectron Spectroscopy. The chemical states of carbon/oxygen/silicon atoms in nanocomposites is shown by C 1s, O 1s, and Si 2sp X-ray photoelectron spectroscopy (XPS) spectra in Figure 3. Table 1 presents the elemental composition (C, O, and Si), quantification (atom %) and the weight percentage (wt %) obtained from XPS measurements. Quantificational analysis of C, O, and Si in MWCNT composites are explained in terms of the data presented in Table 1. It can be observed from the table that carbon/oxygen atoms are replaced/substituted by oxidized Si-NPs atoms. C 1s, O 1s, and Si 2sp XPS spectra were deconvoluted into different Gaussian lines (see Figure 3), and their different parameters are tabulated in Table 3. C 1s peak observed at ~283.5/284.4 eV (peak I/peak II) for MWCNTs in Figure 3b is assigned to the C═C bond (carbon sp^2-hybridization). This peak is shifted toward higher energy at ~285.3 eV for the low concentration of oxidized Si-NPs (1.5 atom %) deposited MWCNTs and is shown in Figure 3c. This peak is known as a "defect peak"[35] or a Si−C−O bonding peak,[36] indicating a change in structural and electronic behavior of the composites due to SiO_2-NPs deposition. The peaks at 288.8/289.5 eV for MWCNTs and MWCNTs/SiO_2-NPs (Si-NPs = 1.5 atom %), arise from >C−O/−COOH bonds and/or along with Si bonds. The C 1s peak of oxidized Si-NPs decorated MWCNTs shifts towards a lower energy, significantly indicating the formation of sp^3-rich material. The deconvoluted C 1s XPS peaks of MWCNTs/SiO_2-NP (Si-NPs = 5.75 atom %) nanocomposites are observed at ~281.8 and ~282.4 eV which are strong indicators of the C−Si bonds,[37] and confirm the formation of MWCNTs/SiO_2-NP nanocomposites.

MWCNTs spectrum shows two de-convoluted O 1s peaks at 530.5 and at 531.9 eV assigned to C═O and C−O, respectively. The two subpeaks at 533.3 and 532.7 eV for

Table 3. Deconvoluted C 1s, O 1s, and Si 2p XPS Results of SiO_2-NPs, MWCNTs, MWCNTs/SiO_2-NPs (Si-NPs = 1.5 atom %) and MWCNTs/SiO_2-NPs (Si-NPs = 5.75 atom %)

	x (eV)	$\Delta\omega$ (eV)	int. (au)	x (eV)	$\Delta\omega$ (eV)	int. (au)	x (eV)	$\Delta\omega$ (eV)	int. (au)	x (eV)	$\Delta\omega$ (eV)	int. (au)	x (eV)	$\Delta\omega$ (eV)	int. (au)	
C 1s and O 1s XPS	Peak-I (C═C/C−Si)			Peak-II (C═C)			Peak-III (C−O−Si/−COOH−Si)			Peak-I (C═O)			Peak-II (C−O)			
MWCNTs	283.5	0.7	48.7	284.3	2.3	25.0	288.8	6.5	26.3	530.5	2.7	60.6	531.9	2.2	39.4	
MWCNTs/SiO_2-NPs (Si-NPs = 1.5 atom %)	284.4	0.7	49.4	285.3	2.2	24.7	289.5	6.2	25.8	531.5	2.3	56.2	533.0	2.0	43.8	
MWCNTs/SiO_2-NPs (Si-NPs = 5.75 atom %)	281.8	0.9	87.8	282.4	2.4	12.2				529.2	1.2	67.6	529.8	2.1	32.4	
Si 2s and Si 2p XPS	Peak-I (Si−Si)			Peak-II (Si−Si)			Peak-III (Si−Si)			I = Si−C/Si−C−O/Si−O			II = Si−C/Si−C−O/Si−O			
SiO_2-NPs	150.7	4.4	375	151.9	1.7	389	153.1	3.4	259	101.2	1.3	7241	100.8	1.2	7689	
MWCNTs/SiO_2-NPs (Si-NPs = 1.5 atom %)	151.6	2.3	270	154.1	2.2	588	156.3	4.9	142	100.4	3.1	28.0	103.0	2.4	72.0	
MWCNTs/SiO_2-NPs (Si-NPs = 5.75 atom %)	148.6	2.1	231	150.6	1.5	1224	151.6	2.9	851	99.4	1.2	60.0	100.2	2.1	40.0	

DOI: 10.1021/acsomega.9b01958
ACS Omega 2019, 4, 14589−14598

MWCNTs/SiO_2-NP nanocomposites are due to the O−C and O−Si groups, respectively.[38] The Si 2p and 2s XPS spectra of Figure 3i show the main peaks at ∼100 and ∼150 eV, respectively, for Si-NPs. These XPS spectra for Si 2p and 2s are also observed in Figure 3j−l for MWCNTs/SiO_2-NP nanocomposites with different peak positions. Different decomposed peaks between ∼99.0 and 102 eV for Si 2p are assigned to Si−C/Si−C−O and that at ∼103.0 eV to Si−O.[37−39] The peaks at ∼151.1−153.0 eV range for Si 2s XPS spectra are Si−Si peaks and those above 153.0 eV are assigned to Si−O.[40] These results clearly indicate that SiO_2-NPs are responsible for the change in the electronic and bonding structure of the MWCNT/SiO_2-NP composites. Based on the XPS decomposed peak intensity, it can be hypothesized that SiO_2-NPs are responsible for the change in structural properties of MWCNTs and can make a material rich in sp^3. This hypothesis is confirmed by the data acquired from the Raman spectra.

2.6. Current−Voltage (*I*−*V*) Measurement. Figure 4a shows that the ohmic *I*−*V* relationship is more pronounced for

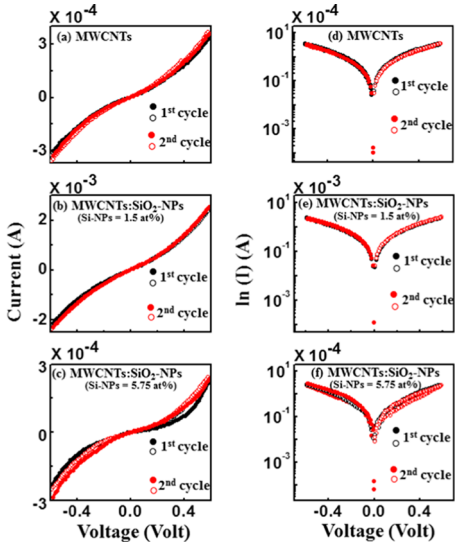

Figure 4. (a−c) Current (*I*)−voltage (*V*) linear and (d−f) (ln *I*−*V*) relationships of MWCNTs, MWCNTs/SiO_2-NP (Si-NPs = 1.5 atom %) nanocomposites, and MWCNTs/SiO_2-NP (Si-NPs = 5.75 atom %) nanocomposites, respectively [there are two cycles measurements of (*I*−*V*) and (ln *I*−*V*) for each case].

MWCNT. The results in Figure 4b,c also show that in MWCNTs, SiO_2-NPs are responsible for the change in conductivity of the composites. As the concentration of the deposited SiO_2-NPs increases, the *I*−*V* tends to deviate from ohmic to nonohmic behavior with a slight decrease in the electrical conductivity of the composites from conducting to semiconducting. The increase in conductivity of MWCNTs/SiO_2 (Si-NPs = 1.5 atom %) is due to a dangling bond formed in MWCNTs due to decreased silicon content.[41] The bond creates levels in the forbidden gap of the material that generate charge carriers to contribute to the measured current. On the other hand, a slight decrease in the electrical conductivity may be due to the change in the electrical structure of MWCNTs. The *I*−*V* hysteresis loops for MWCNTs and MWCNTs/SiO_2-NP nanocomposites are shown in Figure 4d−f. Unlike in the case of MWCNTs and MWCNTs/SiO_2-NPs (Si-NPs = 1.5 atom %), a small *I*−*V* hysteresis loop is observed for MWCNTs/SiO_2-NPs (Si-NPs = 5.75 atom %), indicating a charge storage property of these composites. The loop area of the first cycle is higher than that of the second cycle, signifying a Coulombic blockade and an electron−hole recombination, which is consistent with the silicon single-electron transistor.[42] Figure 4e,f shows that the loop for MWCNTs/SiO_2-NPs (Si-NPs = 5.75 atom %) has an area larger than that for the MWCNTs/SiO_2-NPs (Si-NPs = 1.5 atom %). The larger hysteresis loop indicates that the material has a high charge storage behavior. Based on the current (conductivity) variation of MWCNTs with the oxidized Si-NPs concentration, we can hypothesize that the material could be useful for ferroelectric device applications.

2.7. *M*−*H* Hysteresis Loops. The magnetic-field-dependent *M*−*H* hysteresis loops of the synthesized composites are presented in Figure 5a−d. In Figure 5a,b, a paramagnetic behavior is observed for SiO_2-NPs, whereas pure MWCNTs show a ferromagnetic behavior. Considering Figure 5c,d, the magnetization of MWCNTs/SiO_2-NPs (Si-NPs = 1.5 atom %) increases slightly but decreases for MWCNTs/SiO_2-NP (Si-NPs = 5.75 atom %) nanocomposites. These results indicate that ferromagnetic behavior gets suppressed as the concentration of SiO_2-NPs in MWCNTs increase. The hysteresis loops measured at 40 and 300 K are used to explain this variation of the magnetization, and different magnetization parameters are tabulated in Table 4. The structural change of MWCNTs can be explained in terms of variation of magnetization (M_S). The reduction of M_S is due to the formation of Si−C bonding along with Si−O, making the material rich in sp^3. The interaction of silicon atoms with other elements in MWCNTs has been explained elsewhere with possibilities of reducing sp^2 while increasing sp^3 hybridization.[40,43]

2.8. Zero Field Cooling and Field Cooling. The temperature dependence of zero field cooling (ZFC) and field cooling (FC) measurements of SiO_2-NPs, MWCNTs, and MWCNTs/SiO_2-NPs are presented in Figure 5e−g. The figure shows that MWCNTs and MWCNTs/SiO_2-NPs have ferromagnetic features and thus are in agreement with the ferromagnetic behavior observed in the *M*−*H* hysteresis loops. This study reveals that the oxidized Si-NPs are responsible for the semiconducting magnetic behavior of MWCNTs. This ability to control the structural behavior of MWCNTs by manipulating their structure opens new vistas for more electronic and spintronic devices. As a low toxicity material, the ability to control the properties of MWCNTs also gives room for applications in biomedicine.

2.9. Electron Spin Resonance. Figure 5i−l shows the ferromagnetism behavior of the nanocomposites using electron spin resonance (ESR) technique at room temperature. A prominent resonant microwave absorption signal (H_r) is observed at around 3200 G/1600 G for high/low field in the figure. The linewidth (ΔH) of ESR signals are 367/203, 433/190, 711/117, and 1284/148 for Si-NPs, MWCNTs, MWCNTs/SiO_2-NPs (Si-NPs = 1.5 atom %), and MWCNTs/SiO_2-NPs (Si-NPs = 5.75 atom %) in high/low field, respectively. Parameters calculated from the ESR spectra are presented in Table 5. The *g*-value (Landé *g* factor) or $\Delta g/g$ value changes with the deposition of SiO_2-NPs on MWCNTs surface. From Table 5, the linewidth with an effective *g* value for MWCNTs/SiO_2-NP (Si-NPs = 1.5 atom %) nanocomposites is higher than that for pure SiO_2-NPs, MWCNTs, and MWCNTs/SiO_2-NPs (Si-NPs = 5.75 atom %), indicating that MWCNTs/SiO_2-NPs (Si-NPs = 1.5 atom %) have a

DOI: 10.1021/acsomega.9b01958
ACS Omega 2019, 4, 14589−14598

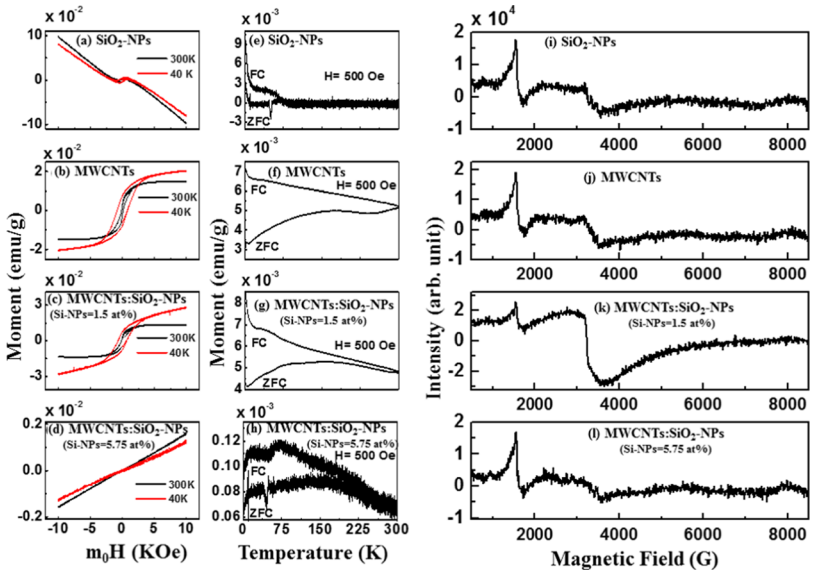

Figure 5. Magnetic hysteresis loops obtained for (a) SiO_2-NPs, (b) MWCNTs, (c) MWCNTs/SiO_2-NP (Si-NPs = 1.5 atom %) nanocomposites, and (d) MWCNTs/SiO_2-NP (Si-NPs = 5.75 atom %) nanocomposites at 300 and 40 K. Temperature dependence of magnetization of (e) SiO_2-NPs, (f) MWCNTs, (g) MWCNTs/SiO_2-NPs (Si-NPs = 1.5 atom %), and (h) MWCNTs/SiO_2-NPs (Si-NPs = 5.75 atom %) with applied magnetic field of 500 Oe after zero field cooling (ZFC) and field cooling (FC). Electron spin resonance spectra for (i) Si-NPs, (j) MWCNTs, (k) MWCNTs/SiO_2-NP (Si-NPs = 1.5 atom %) nanocomposites, and (l) MWCNTs/SiO_2-NP (Si-NPs = 5.75 atom %) nanocomposites at 300 K.

Table 4. Magnetization Parameters [Magnetic Saturation (M_S), Retentivity (M_R), and Coercivity (H_C)] of Si-NPs, MWCNTs, MWCNTs/SiO_2-NPs (Si-NPs = 1.5 atom %) and MWCNTs/SiO_2-NPs (Si-NPs = 5.75 atom %) Obtained from the $M-H$ Hysteresis Loops Measured at 300 and 40 K

	@300 K			@40 K		
magnetization ($M-H$ loops)	$M_S \times 10^{-4}$ (emu/g)	$M_R \times 10^{-4}$ (emu/g)	H_C (Oe)	$M_S \times 10^{-4}$ (emu/g)	$M_R \times 10^{-4}$ (emu/g)	H_C (Oe)
SiO_2-NPs	49	36.0	379	57	43	515
MWCNTs	140	25.0	112	190	73	813
MWCNTs/SiO_2-NPs (Si-NPs = 1.5 atom %)	130	23.0	123	220	76	689
MWCNTs/SiO_2-NPs (Si-NPs = 5.75 atom %)		00.2	60		0.07	357

Table 5. Electron Spin Resonance Parameters of Si-NPs, MWCNTs, MWCNTs/SiO_2-NPs (Si-NPs =1.5 atom %), and MWCNTs/SiO_2-NPs (Si-NPs = 5.75 atom %) Measured at 300 K

	ΔH (Gauss)		H_r (Gauss)		g-value				
magnetization (ESR)	high field	low field	high field	low field	high field	low field	N (no. of spin)	P_{asy}	$\Delta g/g$
SiO_2-NPs	367	203	3243	1673	2.08	4.03	3.67×10^8	0.32	0.0375
MWCNTs	433	190	3298	1680	2.04	4.17	6.11×10^8	0.23	0.0182
MWCNTs/SiO_2-NPs (Si-NPs = 1.5 atom %)	711	117	3198	1572	2.11	4.29	7.54×10^9	0.24	0.0511
MWCNTs/SiO_2-NPs (Si-NPs = 5.75 atom %)	1284	148	3303	1616	2.04	4.11	3.65×10^9	0.56	0.0182

higher magnetic phase in MWCNTs.[44] Similar values have been reported elsewhere for other forms of carbon.[45] A possible overlap of the broad linewidth with resonance line of an unpaired electron that is trapped in an oxygen vacancy in MWCNTs makes H_r to shift toward the lower field for the g-value greater than 2. Majchrzycki et al.[46] have reported similar results on functionalized graphene materials. The asymmetric factor (P_{asy}) was estimated using the relation $P_{asy} = (1 - h_u/h_l)$,[47] where h_u and h_l are the upper and lower peak heights, respectively, from zero line. It was observed that P_{asy} increases gradually with an increase of oxidized Si-NPs content in MWCNTs, as shown in Table 5. The highest magnetic anisotropy was obtained for MWCNTs/SiO_2-NPs (Si-NPs = 1.5 atom %). The total number of spin (N) regarding the ESR resonance was calculated using the following relation: $N = 0.285 \times I_{p-p} \times (\Delta H)^2$,[48] where I_{p-p} is the peak-to-peak height of the ESR signal (in au) and ΔH is the linewidth in Gauss. The $\Delta g/g$ and N values are high in the case of MWCNTs/SiO_2-NPs (Si-NPs = 1.5 atom %) nanocomposites leading to a high value of magnetization. These results confirm that the MWCNTs/SiO_2-NP (Si-NPs = 1.5 atom %) nanocomposites can preserve the magnetism as MWCNTs that could be very useful for electromagnetic applications.

As observed from Raman spectra, the sp^2 content is higher in MWCNTs/SiO_2-NP (Si-NPs = 1.5 atom %) and lower in MWCNTs/SiO_2-NP (Si-NPs = 5.75 atom %) composites than in pure MWCNTs, thereby giving rise to sp^3 content for 5.75 atom % oxidized Si-NP-deposited MWCNTs. This observation is consistent with XPS and XANES data. The XPS spectra for pure MWCNTs show that the sp^2 C═C peak at ∼284.4 eV

DOI: 10.1021/acsomega.9b01958
ACS Omega 2019, 4, 14589−14598

shifted toward a high binding energy, thereby forming a defect peak at 285.3 eV with a decrease in the intensity of the MWCNTs/SiO_2-NPs. This defected peak is ∼0.9 eV higher than that of pure MWCNTs. The weak attachment bond of MWCNTs/SiO_2-NPs (Si-NPs = 1.5 atom %) on the surface of MWCNTs can be attributed to this defected peak. The increase/decrease in the intensity of C K-edge XANES spectra correspond to a increase/decrease in the I_D/I_G ratio, indicating a change in structural/electronic nature of MWCNTs/SiO_2-NPs. The observed change in the structural/electronic properties of MWCNTs due to the deposition of SiO_2-NPs (Si-NPs = 1.5 atom %) content leads to the formation of the Si−C−O and C−O/−COOH bonds due to oxygen (O) vacancy created, which may be responsible for the higher magnetization. The presence of oxygen functional group creates a positive center, which captures an electron in a localized form.[49,50] The local electrons possess magnetic moments that improve the magnetism in MWCNTs/SiO_2-NP (Si-NPs = 1.5 atom %) nanocomposites. The strong interaction (tetrahedral bonding Si−C) between the atoms of Si and C may be responsible for the rapid decrease in the magnetization of MWCNTs due to an increase in the SiO_2-NPs content.[40] The relationship between the electrical and magnetic properties of MWCNT:SiO_2-NPs can be clarified by the transport properties of the MWCNTs/SiO_2-NP nanocomposites. The ferromagnetism induced in MWCNT/SiO_2-NPs was also based on the delocalized electrons not trapped by O vacancy.[50] The magnetic and electrical properties are mainly due to the mobility of electrons between the atoms. The delocalized electrons allow for easy transition between the valence and the conduction bands, leading to an enhancement in electrical conductivity.[51] In addition, the delocalized electrons also enhance the exchange interaction of atoms, which eventually improves the ferromagnetic behavior of MWCNT/SiO_2-NP nanocomposites.[50,52]

3. CONCLUSIONS

The electrical, electronic, and magnetic behaviors of the synthesized MWCNTs and MWCNTs/SiO_2-NP nanocomposites have been investigated. We observed that there is a change in the structure of MWCNTs from sp^2- to sp^3-rich hybridized carbon atoms with a change in the electrical conductivity of MWCNTs due to the deposition/decoration of SiO_2-NPs on the surface of MWCNTs. The formation of Si−C, Si−Si, and Si−O−C/Si−O bonding features was observed, indicating that SiO_2-NPs impacted the chemical bonding and electronic structure of MWCNTs. The magnetization of MWCNTs varies as a function of oxidized Si-NPs content adhered onto the surface of MWCNTs lattice. We therefore conclude that the deposition/decoration of oxidized Si-NPs on the surface of MWCNTs is an alternative method to tailor the structural, electrical, and magnetic properties of MWCNTs for future electronic and magnetic device applications.

4. EXPERIMENTAL DETAILS

4.1. Synthesis Process. Spray pyrolysis process was used to prepare MWCNTs using a solution of ferrocene ($C_{10}H_{10}Fe$ as a catalyst) and toluene (C_7H_8 as a carbon source),[53] whereas thermal decomposition process was used for the synthesis of silicon nanoparticles (SiO_2-NPs) using chloro-(dimethyl) octadecylsilane in 1,3,5-trimethylbenzene in the presence of octadecylamine.[54] Since the synthesis process of the nanocomposites was carried out in an atmospheric pressure, Si-NPs were oxidized to form SiO_2-NP. For the preparation of MWCNT:SiO_2-NPs composites, we used SiO_2-NPs and MWCNTs at two different stoichiometric ratios (Si-NPs = 1.5 atom % and Si-NPs = 5.75 atom %), which were suspended in toluene and heated at above 100 °C to obtain MWCNTs/SiO_2-NP nanocomposites. The deposited SiO_2-NPs have been found to be possibly deposited on the MWCNTs matrices.

4.2. Measurements. SiO_2-NPs, MWCNTs, and MWCNTs/SiO_2-NP nanocomposites were characterized by the use of different techniques to establish and study the change in their surface morphology, microstructure, electronic, and magnetic properties due to the deposition of SiO_2-NPs in the MWCNT lattice. The deposited SiO_2-NPs on MWCNTs were denoted as MWCNTs/SiO_2-NPs (Si-NPs = 1.5 atom %) and MWCNTs/SiO_2-NPs (Si-NPs = 5.75 atom %) translating to 1.5% and 5.57 atom % of Si-NPs concentration in MWCNTs, respectively. The SiO_2-NPs, MWCNTs, and MWCNTs/SiO_2-NPs was drop-cast on a silicon substrate and air-dried overnight prior to measurements. All measurements were performed at room temperature except magnetic measurements. To obtain the surface morphology of SiO_2-NPs, MWCNTs, and MWCNTs/SiO_2-NP nanocomposites, field emission scanning electron microscopy (FESEM) images were recorded using a JSM-7800F FESEM from JEOL Ltd. coupled with an UltraDry EDS detector. The structural studies of the synthesized composites were performed using a Rigaku Smartlab X-ray diffractometer (0.154 nm Cu Kα line). Raman spectra were recorded using a HORIBA scientific XploRA at 532 nm (∼2.41 eV) LASER light excitation energy. The surface morphological structures were studied using JEOL JEM 2100. The C K-edge, O K-edge, and Si $L_{3,2}$-edge XANES measurements were performed at the Taiwan Light Source (TLS), Hsinchu, Taiwan. The core shells C 1s, O 1s, and Si 2sp were performed using a KRATOS-SUPRA spectrometer with a monochromatic Al Kα radiation possessing an excitation energy, $h\nu$ = 1486.6 eV, and a base pressure 1.2×10^{-9} Torr at UNISA (Florida Science Campus). The electrical conductivity was studied using Keithley 6487 with a voltage sweep ranging from −0.6 to +0.6 V. In this measurements, silver paste was used as the conducting electrodes to investigate the electrical behavior of the materials. The range voltage of 0−+0.6 V, +0.6−0 V, 0−−0.6 V, and −0.6−0 V was used to obtain the $I-V$ data. The value of 0.6 V was the highest voltage applied for the current limit of 2.5 mA. A SQUID-type magnetometer with a sensitivity of $<5 \times 10^{-8}$ emu was used for the $M-H$ loop and FC/ZFC measurements. All the measurements were performed at room temperature. Electron spin resonance (ESR) spectra were recorded using a Bruker EMX spectrometer at 9.45 GHz. Details of these measurement techniques are available elsewhere.[55]

AUTHOR INFORMATION

Corresponding Authors

*E-mail: Raysc@unisa.ac.za.
*E-mail: wfpong@mail.tku.edu.tw.

ORCID

Sekhar C. Ray: 0000-0003-3202-4739

Notes

The authors declare no competing financial interest.

DOI: 10.1021/acsomega.9b01958
ACS Omega 2019, 4, 14589−14598

■ ACKNOWLEDGMENTS

The financial support received from the National Research Foundation (NRF), South Africa (Grant nos. 105292, PD-TWAS150813137166, and EQP13091742446) is gratefully acknowledged by J.A.O., D.O.I., S.J.M., S.S., and S.C.R.

■ REFERENCES

(1) Iijima, S. Helical microtubules of graphitic carbon. *Nature* **1991**, *354*, 356.
(2) Gao, C.; Guo, Z.; Liu, J. H.; Huang, X. J. The new age of carbon nanotubes: an updated review of functionalized carbon nanotubes in electrochemical sensors. *Nanoscale* **2012**, *4*, 1948−1963.
(3) Zhang, N.; Yang, M.-Q.; Liu, S.; Sun, Y.; Xu, Y.-J. Waltzing with the Versatile Platform of Graphene to Synthesize Composite Photocatalysts. *Chem. Rev.* **2015**, *115*, 10307−10377.
(4) Chen, Y.; Xie, X.; Xin, X.; Tang, Z.-R.; Xu, Y.-J. Ti3C2T X-Based Three-Dimensional Hydrogel by a Graphene Oxide-Assisted Self-Convergence Process for Enhanced Photoredox Catalysis. *ACS Nano* **2019**, *13*, 295−304.
(5) Zhang, N.; Zhang, Y.; Yang, M.-Q.; Tang, Z.-R.; Xu, Y.-J. A Critical and Benchmark Comparison on Graphene-, Carbon Nanotube-, and Fullerene-Semiconductor Nanocomposites as Visible Light Photocatalysts for Selective Oxidation. *J. Catal.* **2013**, *299*, 210−221.
(6) Adjizian, J. J.; Leghrib, R.; Koos, A. A.; Suarez-Martinez, I.; Crossley, A.; Wagner, P.; Grobert, N.; Llobet, E.; Ewels, C. P. Boron- and nitrogen-doped multi-wall carbon nanotubes for gas detection. *Carbon* **2014**, *66*, 662−673.
(7) Baierle, R. J.; Fagan, S. B.; Mota, R.; da Silva, A. J.; Fazzio, A. Electronic and structural properties of silicon-doped carbon nanotubes. *Phys. Rev. B* **2001**, *64*, No. 085413.
(8) Song, C.; Xia, Y.; Zhao, M.; Liu, X.; Li, F.; Huang, B.; Zhang, H.; Zhang, B. Functionalization of silicon-doped single walled carbon nanotubes at the doping site: an ab initio study. *Phys. Lett. A* **2006**, *358*, 166−170.
(9) Meric, I.; Han, M. Y.; Young, A. F.; Ozyilmaz, B.; Kim, P.; Shepard, K. L. Current saturation in zero-bandgap, top-gated graphene field-effect transistors. *Nat. Nanotechnol.* **2008**, *3*, 654.
(10) Slepyan, G. Y.; Maksimenko, S. A.; Lakhtakia, A.; Yevtushenko, O.; Gusakov, A. V. Electrodynamics of carbon nanotubes: Dynamic conductivity, impedance boundary conditions, and surface wave propagation. *Phys. Rev. B* **1999**, *60*, No. 17136.
(11) Pennington, G.; Goldsman, N. Semiclassical transport and phonon scattering of electrons in semiconducting carbon nanotubes. *Phys. Rev. B* **2003**, *68*, No. 045426.
(12) Daenen, M.; De Fouw, R. D.; Hamers, B.; Janssen, P. G.; Schouteden, K.; Veld, M. A. *The Wondrous World of Carbon Nanotubes—A Review of Current Carbon Nanotube Technologies*; Eindhoven University of Technology, 2003; pp 1−96.
(13) Atchudan, R.; Pandurangan, A.; Joo, J. Effects of nanofillers on the thermo-mechanical properties and chemical resistivity of epoxy nanocomposites. *J. Nanosci. Nanotechnol.* **2015**, *15*, 4255−4267.
(14) Zhang, X.; Fu, J.; Zhang, Y.; Lei, L. A nitrogen functionalized carbon nanotube cathode for highly efficient electrocatalytic generation of H_2O_2 in Electro-Fenton system. *Sep. Purif. Technol.* **2008**, *64*, 116−123.
(15) Ciomaga, C. E.; Padurariu, L.; Curecheriu, L. P.; Lupu, N.; Lisiecki, I.; Deluca, M.; Tascu, S.; Galassi, C.; Mitoseriu, L. Using multi-walled carbon nanotubes in spark plasma sintered Pb$(Zr_{0.4}7Ti_{0.53})O_3$ ceramics for tailoring dielectric and tunability properties. *J. Appl. Phys.* **2014**, *116*, No. 164110.
(16) Casati, R.; Hamidi Nasab, M.; Coduri, M.; Tirelli, V.; Vedani, M. Effects of Platform Pre-Heating and Thermal-Treatment Strategies on Properties of $AlSi_{10}Mg$ Alloy Processed by Selective Laser Melting. *Metals* **2018**, *8*, No. 954.
(17) Svavarsson, H. G.; Arnardottir, H.; Einarsson, S.; Albertsson, A.; Brynjolfsdottir, A. In *Applications of Unmodified Geothermal Silica for Protein Extraction*, Proceedings of the World Geothermal Congress, Melbourne, Australia, 2015; pp 1−8.
(18) Senez, V.; Armigliato, A.; De Wolf, I.; Carnevale, G. P.; Balboni, R.; Frabboni, S.; Benedetti, A. Strain Determination in Silicon Microstructures by Combined TEM/CBED, Process Simulation and micro-Raman Spectroscopy. *J. Appl. Phys.* **2003**, *94*, 5574−5583.
(19) Ferrari, A. C.; Robertson, J. Interpretation of Raman spectra of disordered and amorphous carbon. *Phys. Rev. B* **2000**, *61*, No. 14095.
(20) Ray, S. C.; Bhunia, S. K.; Saha, A.; Jana, N. R. Electric and Ferro-electric behaviour of polymer-coated graphene-oxide thin film. *Phys. Procedia* **2013**, *46*, 62−70.
(21) Ferrari, A. C.; Basko, D. M. Raman spectroscopy as a versatile tool for studying the properties of graphene. *Nat. Nanotechnol.* **2013**, *8*, 235.
(22) Soin, N.; Roy, S. S.; Ray, S. C.; McLaughlin, J. A. Excitation energy dependence of Raman bands in multiwalled carbon nanotubes. *J. Raman Spectrosc.* **2010**, *41*, 1227−1233.
(23) Murphy, H.; Papakonstantinou, P.; Okpalugo, T. T. Raman study of multiwalled carbon nanotubes functionalized with oxygen groups. *J. Vac. Sci. Technol., B: Microelectron. Nanometer Struct. Process., Meas., Phenom.* **2006**, *24*, 715−720.
(24) Moene, R.; Makkee, M.; Moulijn, J. A. High surface area silicon carbide as catalyst support characterization and stability. *Appl. Catal., A* **1998**, *167*, 321−330.
(25) Tarui, T.; Takahashi, T.; Ohashi, S.; Uemori, R. In *Effect of Silicon on the Age Softening of High Carbon Steel Wire*, Proceedings of the 35th Mechanical Working and Steel Processing Conference; Iron & Steel Society of AIME, 1993; pp 231−239.
(26) Jin, Y. Z.; Gao, C.; Hsu, W. K.; Zhu, Y.; Huczko, A.; Bystrzejewski, M.; Roe, M.; Lee, C. Y.; Acquah, S.; Kroto, H.; Walton, D. R. Large-scale synthesis and characterization of carbon spheres prepared by direct pyrolysis of hydrocarbons. *Carbon* **2005**, *43*, 1944−1953.
(27) Tuinstra, F.; Koenig, J. L. Raman spectrum of graphite. *J. Chem. Phys.* **1970**, *53*, 1126−1130.
(28) Pao, C. W.; Ray, S. C.; Tsai, H. M.; Chen, Y. S.; Chen, H. C.; Lin, I. N.; Pong, W. F.; Chiou, J. W.; Tsai, M. H.; Shang, N. G.; Papakonstantinou, P.; Guo, J.-H. Change of structural behaviors of organo-silane exposed graphene nanoflakes. *J. Phys. Chem. C* **2010**, *114*, 8161−8166.
(29) Ray, S. C.; Pao, C. W.; Tsai, H. M.; Chiou, J. W.; Pong, W. F.; Chen, C. W.; Tsai, M. H.; Papakonstantinou, P.; Chen, L. C.; Chen, K. H. A comparative study of the electronic structures of oxygen-and chlorine-treated nitrogenated carbon nanotubes by x-ray absorption and scanning photoelectron microscopy. *Appl. Phys. Lett.* **2007**, *91*, No. 202102.
(30) Terekhov, V. A.; Terukov, E. I.; Trapeznikova, I. N.; Kashkarov, M.; Kurilo, O. V.; Turishchev, S. Y.; Golodenko, A. B.; Domashevskaya, E. P. A study of the local electronic and atomic structure in a-Si_xC_{1-x} amorphous alloys using ultrasoft X-ray emission spectroscopy. *Semiconductors* **2005**, *39*, 830−834.
(31) Banerjee, S.; Hemraj-Benny, T.; Balasubramanian, M.; Fischer, D. A.; Misewich, J. A.; Wong, S. S. Ozonized single-walled carbon nanotubes investigated using NEXAFS spectroscopy. *Chem. Commun.* **2004**, 772−773.
(32) Stöhr, J. *NEXAFS Spectroscopy*; Springer Science+Business Media, 2013.
(33) Wu, Z. Y.; Jollet, F.; Seifert, F. Electronic structure analysis of via x-ray absorption near-edge structure at the Si K, and OK edges. *J. Phys.: Condens. Matter* **1998**, *10*, 8083.
(34) Mo, S. D.; Ching, W. Y. X-ray absorption near-edge structure in alpha-quartz and stishovite: Ab initio calculation with core−hole interaction. *Appl. Phys. Lett.* **2001**, *78*, 3809−3811.
(35) Shang, N. G.; Papakonstantinou, P.; McMullan, M.; Chu, M.; Stamboulis, A.; Potenza, A.; Dhesi, S. S.; Marchetto, H. Catalyst-free efficient growth, orientation and biosensing properties of multilayer graphene nanoflake films with sharp edge planes. *Adv. Funct. Mater.* **2008**, *18*, 3506−3514.
(36) Maruyama, T.; Naritsuka, S. *Nanotechnology and Nanomaterials: Carbon Nanotubes—Synthesis, Characterization, Applications*, In Yellampalli, S., Ed.; Department of Material Science and Engineering,

DOI: 10.1021/acsomega.9b01958
ACS Omega 2019, 4, 14589−14598

Meijo University: Japan, 2011; https://www.intechopen.com/books/carbon-nanotubes-synthesis-characterization-applications.
(37) Pedio, M.; Borgatti, F.; Giglia, A.; Mahne, N.; Nannarone, S.; Giovannini, S.; Cepek, C.; Magnano, E.; Bertoni, G.; Spiller, E.; Sancrotti, M.; Giovanelli, L.; Floreano, L.; Gotter, R.; Morgante, A. Annealing temperature dependence of C60 on silicon surfaces: bond evolution and fragmentation as detected by NEXAFS. *Phys. Scr.* **2005**, *2005*, No. 695.
(38) Moulder, J. F.; Stickle, W. F.; Sobol, P. E. *KD Bomben Handbook of X-Ray Photoelectron Spectroscopy: A Reference Book of Standard Spectra for Identification and Interpretation of XPS Data*; Electro Inc.: USA, 1992; p 42.
(39) Deng, H. X.; Wei, S. H.; Li, S. S.; Li, J.; Walsh, A. Electronic origin of the conductivity imbalance between covalent and ionic amorphous semiconductors. *Phys. Rev. B* **2013**, *87*, No. 125203.
(40) Ray, S. C.; Mishra, D. K.; Strydom, A. M.; Papakonstantinou, P. Magnetic behavioural change of silane exposed graphene nanoflakes. *J. Appl. Phys.* **2015**, *118*, No. 115302.
(41) Račiukaitis, G.; Brikas, M.; Kazlauskienė, V.; Miškinis, J. Doping of silicon with carbon during laser ablation process. *Appl. Phys. A* **2006**, *85*, 445−450.
(42) Fujiwara, A.; Takahashi, Y.; Murase, K. Observation of single electron-hole recombination and photon-pumped current in an asymmetric Si single-electron transistor. *Phys. Rev. Lett.* **1997**, *78*, No. 1532.
(43) Mostafa, M.; Banerjee, S. Effect of functional group topology of carbon nanotubes on electrophoretic alignment and properties of deposited layer. *J. Phys. Chem. C* **2014**, *118*, 11417−11425.
(44) Rao, S. S.; Stesmans, A.; Noyen, J. V.; Jacobs, P.; Sels, B. ESR evidence for disordered magnetic phase from ultra-small carbon nanotubes embedded in zeolite nanochannels. *Europhys. Lett.* **2010**, *90*, No. 57003.
(45) Gerstner, E. G.; Lukins, P. B.; McKenzie, D. R.; McCulloch, D. G. Substrate bias effects on the structural and electronic properties of tetrahedral amorphous carbon. *Phys. Rev. B* **1996**, *54*, No. 14504.
(46) Majchrzycki, Ł.; Augustyniak-Jabłokow, M. A.; Strzelczyk, R.; Maćkowiak, M. Magnetic Centres in Functionalized Graphene. *Acta Phys. Pol., A* **2015**, *127*, No. 540.
(47) Das, J.; Mishra, D. K.; Srinivasu, V. V. Spin canting and magnetism in nano-crystalline $Zn_{1-x}Al_xO$. *J. Alloys Compd.* **2017**, *704*, 237−244.
(48) Bleaney, B.; Rubins, R. S. Explanation of some Forbidden Transitions in Paramagnetic Resonance. *Proc. Phys. Soc.* **1961**, *77*, 103.
(49) Ghosh, B.; Ray, S. C.; Pattanaik, S.; Sarma, S.; Mishra, D. K.; Pontsho, M.; Pong, W. F. Tuning of the electronic structure and magnetic properties of xenon ion implanted zinc oxide. *J. Phys. D: Appl. Phys.* **2018**, *51*, No. 095304.
(50) Wu, T.; Sun, H.; Hou, X.; Liu, L.; Zhang, H.; Zhang, J. Significant room-temperature ferromagnetism in porous TiO_2 thin films. *Microporous Mesoporous Mater.* **2014**, *190*, 63−66.
(51) Shuai, Z.; Wang, L.; Li, Q. Evaluation of Charge Mobility in Organic Materials: From Localized to Delocalized Descriptions at a First-Principles Level. *Adv. Mater.* **2011**, *23*, 1145−1153.
(52) Ohno, H. Making nonmagnetic semiconductors ferromagnetic. *Science* **1998**, *281*, 951−956.
(53) Vatanpour, V.; Madaeni, S. S.; Moradian, R.; Zinadini, S.; Astinchap, B. Fabrication and characterization of novel antifouling nanofiltration membrane prepared from oxidized multiwalled carbon nanotube/polyethersulfone nanocomposite. *J. Membr. Sci.* **2011**, *375*, 284−294.
(54) Das, P.; Saha, A.; Maity, A. R.; Ray, S. C.; Jana, N. R. Silicon nanoparticle based fluorescent biological label via low temperature thermal degradation of chloroalkylsilane. *Nanoscale* **2013**, *5*, 5732−5737.
(55) Idisi, D. O.; Ali, H.; Oke, J. A.; Sarma, S.; Moloi, S. J.; Ray, S. C.; Wang, H. T.; Jana, N. R.; Pong, W. F.; Strydom, A. M. Electronic, electrical and magnetic behaviours of reduced graphene-oxide functionalized with silica coated gold nanoparticles. *Appl. Surf. Sci.* **2019**, *483*, 106−113.

DOI: 10.1021/acsomega.9b01958
ACS Omega 2019, 4, 14589−14598